IEEE Access
Multidisciplinary ⋮ Rapid Review ⋮ Open Access Journal

Received 16 October 2023, accepted 30 October 2023, date of publication 2 November 2023, date of current version 8 November 2023.

Digital Object Identifier 10.1109/ACCESS.2023.3329933

RESEARCH ARTICLE

Early Performance Degradation Detecting Method for PMSM Based on Change in Frequency Domain Features of Three-Phase Stator Current

QINGCHUAN HE[1], JUN PAN[1], AND XIAOTIAN LYU[2]

[1]National and Local Joint Engineering Research Center of Reliability Analysis and Testing for Mechanical and Electrical Products, Zhejiang Sci-Tech University, Hangzhou 310018, China

[2]Zhejiang CHR Intelligent Equipment Co., Ltd., Jinyun 321404, China

Corresponding authors: Jun Pan (panjun@zstu.edu.cn) and Qingchuan He (heqingchuan@zstu.edu.cn)

This work was supported in part by the Pioneer and Leading Goose Research and Development Program of Zhejiang under Grant 2023C01066, in part by the Special Support Plan for High-Level Talents in Zhejiang Provincial under Grant 2021R52036, and in part by the Manufacturing Processing Equipment of Key Parts used for Civil Aircraft Engine under Grant TC220H05.

ABSTRACT Detect early performance degradation of permanent magnet synchronous motor (PMSM) is very meaningful for preventive maintenance and avoiding catastrophe failure. By fully taking into account effects of rotor flux harmonics and stator current harmonics on electromagnetic torque under actual working condition, a theoretical expression of electromagnetic torque was developed which was used to indirectly evaluate torque ripple without torsional sensor. A new health index for detecting performance degradation and its computational method were proposed by considering the different frequency domain features of three-phase stator current. Based on this the method to detect early performance degradation by monitoring changes in health index are proposed. Experimental results show that the change in the proposed health index is consistent with change in the torque ripple ratio over time and the relative deviation is no more than 10.0%. The early performance degradation of PMSM can be accurately identified by the proposed method whenever the health index exceeds the threshold.

INDEX TERMS Permanent magnet synchronous motor (PMSM), performance degradation, fault detection.

I. INTRODUCTION

Permanent magnet synchronous motor (PMSM) is applied in many fields, e.g. electric vehicles, aircrafts, robots. Its performance degradation is inevitable as time goes on [1]. Sometimes performance degradation may quickly propagate into catastrophe failure and then cause downtime, even catastrophic accident. For example, in the field of aerospace and electric vehicle, anything goes wrong with PMSMs may make catastrophic accident. Therefore, detecting early performance degradation of PMSMs is meaningful for preventive maintenance and avoiding catastrophe failure.

The main cause of PMSM degradation involve inter-turn short-circuit of stator phase windings, demagnetization, bearing wear off, and PWM inverters aging [1]. The inter-turn short-circuit produces a great circulating current with excessive heat, and also causes large electromagnetic torque fluctuations and severe mechanical vibrations [2]. Demagnetization cannot be avoided because of a high temperature, large stator currents and aging of magnet itself [3]. The stator current produces a reverse magnetic field that constantly resists the magnetic field of the permanent magnet. This will gradually cause demagnetization after experiencing long-term operation [4]. Demagnetization can increase torque ripple and reduce efficiency. Bearing wear also causes eccentricity referring to inconsistent air gap between rotor and stator [5]. Air gap eccentricity causes additional vibration, noise, torque ripple and so on [6]. When eccentricity is serious enough, it can cause friction between stator and rotor, and then damage both stator and rotor [7]. Overall, even slight performance degradation has a negative effect on operation, and may quickly propagate into catastrophe failure.

The associate editor coordinating the review of this manuscript and approving it for publication was Jinquan Xu.

Research suggests that any form of fault (or severe degradation) can affect change in the amplitude and frequency of harmonic components in stator current [8], [9]. The inter-turn short circuit causes stator current imbalance and amplitude change. Let f_s be the supply frequency, m be a positive integer. Also, p is the number of pole pairs and z is the number of stator slots. The amplitude of harmonics at $f_{sc} = (1 \pm mz/p)f_s$ increases with increased degree of inter-turn short circuit [10]. Demagnetization causes that the distributed magneto motive force (MMF) is not sinusoidal. The harmonic frequencies $f_{dmg} = (1 \pm m/p)f_s$ can be used as characteristic frequencies for demagnetization [3], [11]. The eccentricity cause distortions in flux distribution inside the motor. This, in turn, causes some current harmonics in the stator current. The harmonic frequencies $f_{ec} = (1 \pm (2m-1)/p)f_s$ can be used as the characteristic frequencies [11]. However, the frequencies mentioned above are not fully competent indexes for performance degradation. Different factors such as design characteristics, the winding configuration and load variation, and even the manufacturing errors have noticeable effects on harmonic components [11]. It is difficult to identify early degradation only by reference to harmonic frequencies. It is significant to develop a better health index to evaluate the level of degradation based on change in amplitude and frequency of harmonic components of stator current.

From effect on function point of view, anything goes wrong with PMSM can increase torque ripple, and this, in turn, leads to undesirable acoustic noise, vibrations, speed oscillations [12], [13], [14]. As time goes on, the torque ripple increases until it reaches a value, at which a signal becomes unusable. In most industry, the torque ripple ratio cannot be greater than 5%. Thus, torque ripple ratio is a competent health index for PMSMs. There are direct and indirect method to measure torque ripple ratio [13], [14]. The direct methods depend on a torsional sensor, but a PMSM usually is not coupled with a torsional sensor under actual working condition. Survey papers show that torque ripple can be indirectly estimated by processing measuring current. The torque ripple is caused by deviations from a sinusoidal flux density distribution around the air gap, by deficiencies of feasible winding geometries, and by the variable magnetic reluctance of air gap due to stator slots [12], [13], [14], [15]. Beyond these, the feeding power converter also contributes to torque ripple due to the harmonics in current waveforms and to time-varying delays between commanded and actual current [16], [17]. Lee et al. presented a torque expression used for indirect sensing of dynamic torque signal taking into account high-order rotor flux harmonics [18]. Zeng et al. presented an indirect method without using a mechanical load [19]. Huang et al. presented a total harmonic distortion index used to evaluate torque quality [20]. Gu et al. present presents a method to calculate torque ripple considering current harmonics [21]. However, in [18], [19], [20], and [21], the estimated torque ripple is a percentage of the peak-to-peak value to theoretical reference value. The harmonic frequencies of the three-phase current were not fully considered, especially the characteristic frequencies resulted from inter-turn short-circuit, demagnetization, bearing wear and PWM inverters aging, and so on. The present methods cannot be used to detect early degradation accurately for PMSM.

This paper develops a method to detect early performance degradation for PMSM based on change in frequency domain features of three-phase stator currents. Firstly, a method to estimate the electromagnetic torque ripple was proposed, which fully considered effects of three-phase current harmonic frequencies. Then, a new health index and its computation method are presented, and the method to detect early performance degradation by monitoring changes in the health index are also proposed. Finally, experiments were conducted to verify effectiveness of the proposed method.

II. METHOD

A. COMPUTATIONAL OF ELECTROMAGNETIC TORQUE

The topology of a three-phase inverter-fed PMSM drive system is shown in Fig.1. The PMSM is controlled through closed loop vector control. The switching sequences is 120° to obtain a three-phase symmetrical output. The phase sequence of i_a, i_b, i_c are displaced by $2\pi/3$ in turn. The orientation of rotor flux vector with respect to stator is determined by rotor position and by instantaneous values of electrical currents.

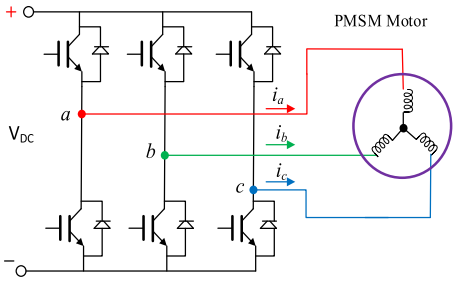

FIGURE 1. PMSM motor drive system.

The theoretical expression of electromagnetic torque is expressed as [22]:

$$T_e = \frac{3}{2}p\left[\Psi_f i_q + (L_\mathrm{d} - L_\mathrm{q})i_\mathrm{d} i_\mathrm{q}\right] \tag{1}$$

where p is the number of pole pairs, Ψ_f represents the part of the flux linkage caused by permanent magnets, L_d and L_q are the d- and q-axis inductances, i_d and i_q are the d- and q-axis currents. In a three-phase PMSM, assuming that the currents have the same amplitude I_m, the same angular frequency ω, the phase currents can be determined by equations:

$$\begin{cases} i_a = I_m \cos(p\omega t + \varphi) \\ i_b = I_m \cos(p\omega t + \varphi - 2\pi/3) \\ i_c = I_m \cos(p\omega t + \varphi + 2\pi/3) \end{cases} \tag{2}$$

Ideally, the sum of current of star-connected windings is equal to zero. However, the actual phase currents are not

perfect sinusoidal, and can be expressed as [23]:

$$\begin{cases} i_a = i_1 \cos(p\omega t + \varphi_1) + \sum_h i_h \cos(hp\omega t + \varphi_h) \\ i_b = i_1 \cos(p\omega t + \varphi_1 - 2\pi/3) \\ + \sum_h i_h \cos(hp\omega t + \varphi_h - 2\pi/3) \\ i_c = i_1 \cos(p\omega t + \varphi_1 + 2\pi/3) \\ + \sum_h i_h \cos(hp\omega t + \varphi_h + 2\pi/3) \end{cases} \tag{3}$$

where h is a positive number, i_1 and φ_1 are the stator current amplitude and phase angle of fundamental wave respectively (the fundamental frequency is also called first harmonic one), i_h and φ_h are the h^{th} harmonic of current amplitude and phase angle respectively. Based on (3), the d- and q-axis currents can be obtained by applying the Blondel-Park transformation:

$$\begin{aligned} &\begin{bmatrix} i_d \\ i_q \end{bmatrix} \\ &= \frac{2}{3}\begin{bmatrix} \cos(p\omega t) & \cos(p\omega t - 2\pi/3) & \cos(p\omega t + 2\pi/3) \\ -\sin(p\omega t) & -\sin(p\omega t - 2\pi/3) & -\sin(p\omega t + 2\pi/3) \end{bmatrix} \\ &\quad \times \begin{bmatrix} i_a & i_b & i_c \end{bmatrix}^T \\ &= \begin{bmatrix} i_1 \cos(\varphi_1) + \sum_h i_h \cos\{(h-1)p\omega t + \varphi_h\} \\ i_1 \sin(\varphi_1) + \sum_h i_h \sin\{(h-1)p\omega t + \varphi_h\} \end{bmatrix} \end{aligned} \tag{4}$$

Usually, the magnetic field of rotor is not perfect sinusoidal distribution in space due to a finite number of slots and effects of manufacturing errors. The distribution can be expressed as superposition of a series of sinusoidal wave [24], [25]. That is, the flux linkages in phase winding should be expressed by:

$$\begin{cases} \Psi_a = \sum_{k=1} \psi_k \cos(kp\theta_k) \\ \Psi_b = \sum_{k=1} \psi_k \cos(kp\theta_k - 2\pi/3) \\ \Psi_c = \sum_{k=1} \psi_k \cos(kp\theta_k + 2\pi/3) \end{cases} \tag{5}$$

where k is a positive number, ψ_k and θ_k are respectively the amplitude and phase of flux linkage harmonics. Based on (5), the d- and q-axis stator flux linkage can be obtained by applying the Blondel-Park transformation:

$$\begin{aligned} &\begin{bmatrix} \Psi_d \\ \Psi_q \end{bmatrix} \\ &= \frac{2}{3}\begin{bmatrix} \cos(p\omega t) & \cos(p\omega t - 2\pi/3) & \cos(p\omega t + 2\pi/3) \\ -\sin(p\omega t) & -\sin(p\omega t - 2\pi/3) & -\sin(p\omega t + 2\pi/3) \end{bmatrix} \\ &\quad \times \begin{bmatrix} \Psi_a & \Psi_b & \Psi_c \end{bmatrix}^T \\ &= \begin{bmatrix} \sum_{k=2} \Psi_k \cos\{(k-1)p\theta\} \\ \sum_{k=2} \Psi_k \sin\{(k-1)p\theta\} \end{bmatrix} \end{aligned} \tag{6}$$

Considering effects of stator current harmonics, the total electromagnetic torque is equal to the sum of contributions of all torque including those generated by current harmonics and flux linkages harmonics. Therefore, expression of the electromagnetic torque becomes:

$$T = \frac{3}{2}p\left[\Psi_f i_q + (L_{\text{d}} - L_{\text{q}})i_{\text{d}}i_{\text{q}} - i_{\text{d}}\Psi_{\text{d}} + i_q\Psi_q\right] \tag{7}$$

When the d- and q-axis inductances are equal to synchronous inductance, that is $L_{\text{d}} = L_{\text{q}}$, the current amplitude i_1 is equal to i_q in case of vector control with $i_d = 0$. With k=1, the fundamental harmonic Ψ_f is equal to Ψ_1. By introducing substitution the Eq.(3) and Eq. (5) in the Eq.(7), the electromagnetic torque is determined by

$$\begin{aligned} T = T^0 + \Delta T^h &= \frac{3}{2}p\psi_1 i_1 \\ &+ \frac{3}{2}p\sum_h \psi_1 i_h \sin\left[(h-1)p\omega t + \varphi_h\right] \\ &+ \frac{3}{2}\sum_{k=2} \psi_k i_1 \cos(\varphi_1)\sin(pk\omega t) \\ &+ \frac{3}{2}\sum_{k=2} \psi_k i_1 \sin(\varphi_1)\cos(pk\omega t) \\ &+ \frac{3}{4}\sum_{k=2}\sum_h \psi_k i_h \sin\left[(k-h+1)p\omega t - \varphi_h\right] \\ &+ \frac{3}{4}\sum_{k=2}\sum_h \psi_k i_h \cos\left[(k+h-1)p\omega t + \varphi_h\right] \end{aligned} \tag{8}$$

where $T^0 = \frac{3}{2}p\psi_1 i_1$ represents electromagnetic torque without considering current harmonics and flux linkage harmonics, $\frac{3}{2}p\sum_h \psi_1 i_h \sin\left[(h-1)\,p\omega t + \varphi_h\right]$ represents the $(h\text{-}1)^{\text{th}}$ torque ripple produced by interaction between the h^{th} current and the 1^{st} flux linkage harmonic. The $\frac{3}{2}\sum_{k=2} \psi_k i_1 \cos\varphi_1 \sin(pk\omega t)$ and $\frac{3}{2}\sum_{k=2} \psi_k i_1 \sin\varphi_1 \cos(pk\omega t)$ represent the k^{th} torque ripple produced by interaction between the 1^{st} current harmonic and the k^{th} flux linkage harmonics, $\frac{3}{4}\sum_{k=2}\sum_h \psi_k i_h \sin\left[(k-h+1)\,p\omega t - \varphi_h\right]$ and $\frac{3}{4}\sum_{k=2}\sum_h \psi_k i_h \cos\left[(k+h-1)\,p\omega t - \varphi_h\right]$ represent the $(k\text{-}h+1)^{\text{th}}$ and $(k+h\text{-}1)^{\text{th}}$ torque ripple reduced by the interaction between the h^{th} current harmonics and the k^{th} flux linkage harmonics, ΔT^h represents the sum of the five terms, except for T^0. By reference to Eq. (8), it takes into account the k^{th} rotor flux harmonics and h^{th} stator current harmonics. The effects of stator current harmonics on electromagnetic torque are fully considered.

B. COMPUTATIONAL METHOD OF HEALTH INDEX

Torque ripple ratio was usually to measure magnitude of torque pulsation during PMSM operation. It refers to the ratio of the maximum amplitude of total torque fluctuation to the average torque when a torsional sensor is used to directly measure torque ripple. The commonly used expression for torque ripple ratio is as follows:

$$K_T = \frac{T_{\max} - T_{\min}}{T_{\text{avg}}} \times 100\% \tag{9}$$

where $T_{\max}$, $T_{\min}$ and T_{avg} are the maximum, minimum and average values of the total torque respectively.

However, the actual T_{max}, T_{min} and T_{avg} can not directly be measured without torsional sensor. During actual measurement process, the amplitude and frequency of harmonic components in the three-phase current are different, especially for the harmonic components. Thus, by reference to Eq.(8), three different torque can be calculated by using the actual measured three-phase current, which are denoted by T_a, T_b, T_c. Let $T_{max} = \max\{T_a, T_b, T_c\}$ repent the maximum among T_a, T_b and T_c, $T_{min} = \min\{T_a, T_b, T_c\}$ repent the minimum among T_a, T_b and T_c, T_{avg} repents the average value of T_a, T_b andT_c. Then, substituting T_{max}, T_{min} and T_{avg} into Eq (10) yields a health index, which can be used to evaluate performance degradation level of the PMSM.

$$K_T = \frac{\max\{T_a, T_b, T_c\} - \min\{T_a, T_b, T_c\}}{(T_a + T_b + T_c)/3} \times 100\% \quad (10)$$

C. EARLY PERFORMANCE DEGRADATION

Supposing that the change in health index is consistent with change in the torque ripple ratio, the early performance degradation can be identified as long as the health index reaches a threshold value, at which a signal becomes unusable. The flowchart of degradation detecting is shown in Fig. 2. Measuring initial health index and determining the threshold value are two critical steps in early performance degradation detection.

The initial health index can be measured as follows. Firstly, measuring electrical parameters (e.g. pole pairs, stator resistance, back-emf) and analyzing the kth rotor flux harmonics. Then, measuring the amplitude and harmonic components in three-phase current under real working conditions. By reference to Eq.(8), calculate the torque T_a, T_b and T_c by using the measured amplitude and harmonic components in three-phase current. By reference to Eq. (10), calculate the initial health index K under specified conditions, such as speed and load.

The threshold value K_f can be measured by using a PMSM with slight performance degradation. In practice, accelerated testing and degradation injection method can be applied to obtain a PMSM with performance degradation in short time. Then, measuring its health index under real working conditions, which will be used as the threshold value for detecting early performance degradation. Once the K_f is determined the performance degradation can be detected in time by following the steps shown in Fig.2.

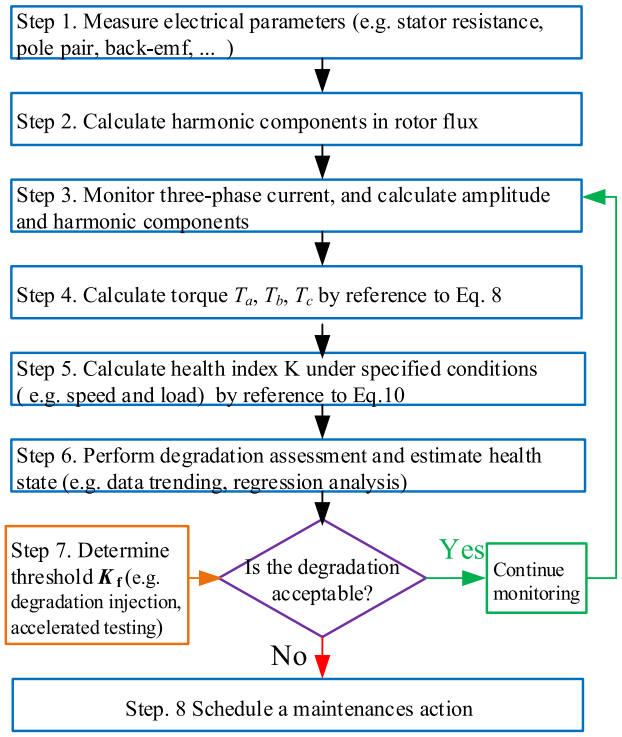

FIGURE 2. Flowchart of performance degradation detecting.

TABLE 1. PMSM parameters.

Parameter	Value
Rated speed	3000 rpm
Rated output power	100 W
Rate torque	0.32 N·m
Magnet pole number	8
Stator winding resistance	1.4 Ω

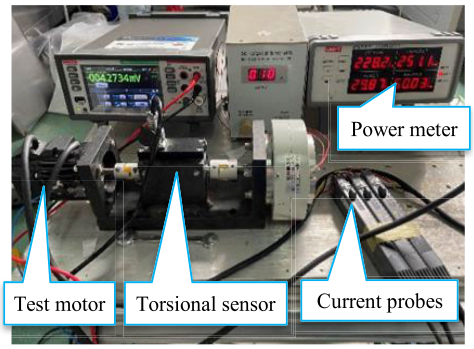

FIGURE 3. Experimental setup.

III. TESTING PROGRESS

A. EXPERIMENT SETUP

Experiments are carried out by using surface-mounted PMSM. The main parameters and specifications are listed in Table 1. the test bench is shown in Fig. 3. The PMSM is coupled with a torsional sensor and a magnetic powder brake. The power consumed by the PMSM is measured by a digital power meter. The phase currents are measured by using current probes with a data acquisition instrument. In this paper, six samples were used to conduct the experiments.

In test 1, a new PMSM was used to test health index under normal conditions. In test 2 and 3, the performance degradation of PWM inverter was infected by using aging MOSFET components which have experienced high temperatures (170°) testing, as shown in Fig.4. When the R_{DS} (drain-source on resistance) increased by about 5% and 15%, we took them from the chamber to simulate the mild extent

and grave performance degradation of PWM inverter, which are named test 2 and 3.

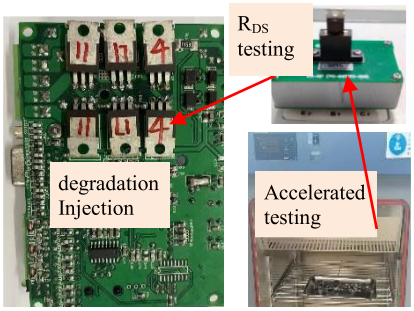

FIGURE 4. Injection of PWM inverter aging.

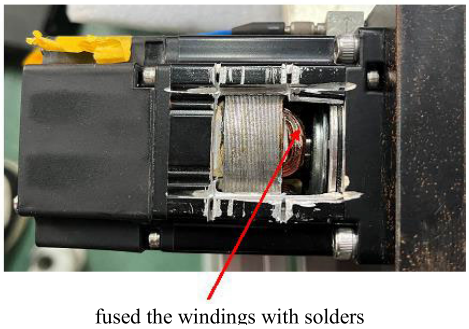

FIGURE 5. Injection of inter-turn short-circuit.

In test 4 and 5, the inter-turn short-circuit was injected by fusing the windings with solders, as shown in Fig.5. The stator winding resistance R_{ab}, R_{bc} and R_{bc} are all 1.4Ω under normal condition. In this paper, we injected two different extent inter-turn short-circuit with $R_{\mathrm{ab}} = 1.3\Omega$ and $R_{\mathrm{ab}} = 1.2\Omega$, which are named test 4 and 5. By comparison with $R_{\mathrm{ab}} = 1.2\Omega$, it is a grave extent of inter-turn short-circuit injection with $R_{\mathrm{ab}} = 1.3\Omega$.

In test 6, a PMSM was tested until measuring torque ripple ratio was greater than 20% with aim to verify the computing method of health index under actual test conditions. The motor nearly always worked under 1800rpm with rated current to accelerate performance degradation. The three-phase current waveforms were measured once a week under different speed and load. The magnetic powder was replaced once a month to keep constant tension. After the test, we completely disassembled the motor and driver to find the problem.

B. TEST BACK-EMF AND CALCULATE FLUX LINKAGES

The back-emf U_{ab}, U_{bc} and U_{ac} are measured at 3000 rpm by using the method given in [26]. The back-emf profile and back-emf spectrums analyzed with fast Fourier transform (FFT) are shown in Fig.6 and Fig.7 respectively. There are no obvious differences among the back-emf spectrums of U_{ab}, U_{bc} and U_{ac}.

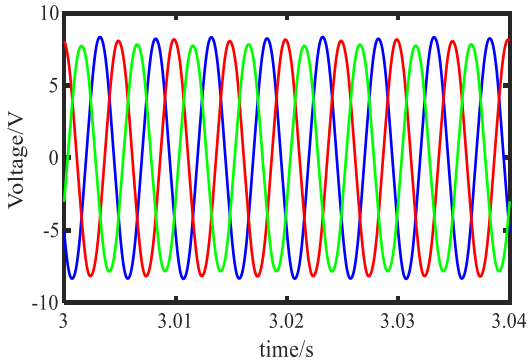

FIGURE 6. Back-emf profile of the tested PMSM.

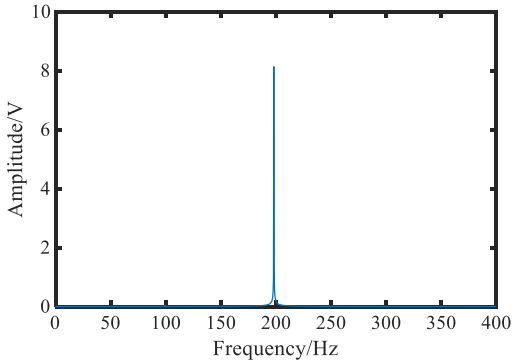

FIGURE 7. Back-emf spectrums of the tested PMSM.

The magnet flux linkage can be derived by:

$$\psi_k = \frac{U_k}{2\sqrt{3}\pi f_r} \tag{11}$$

where U_k (k= 1, 2, 3, 5, 7…) measured in volt is the amplitude of k^{th} harmonic components of the back-emf, f_{r} is rotor rotating frequency measured in hertz, that is $f_{\mathrm{r}} = f_{\mathrm{s}}/\mathrm{p}$. By introducing k^{th} harmonic components substitution to (11), the flux linkages are determined and given in Table 2. The $\bar{\psi}_k$ denotes the average of $\psi_{ab,k}$, $\psi_{bc,k}$ and $\psi_{ac,k}$. By comparison, the amplitude of harmonic is very much smaller than the amplitude of fundamental wave (200 Hz).

TABLE 2. Measuring flux linkages($\times 10^{-2}$ Wb).

Phase	order				
	1	2	3	5	7
$\psi_{ab,k}$	1.536	0. 002	0. 000	0. 001	0. 001
$\psi_{bc,k}$	1.539	0. 001	0. 001	0. 000	0. 000
$\psi_{ac,k}$	1.516	0. 001	0. 005	0. 001	0. 000
$\bar{\psi}_k$	1.529	0.001	0.003	0.001	0.000

IV. RESULT AND DISCUSSION

A. MEASURING RESULTS

Different PMSM (depending on size, power, structure of stator and rotor, control algorithm, and so on) has different

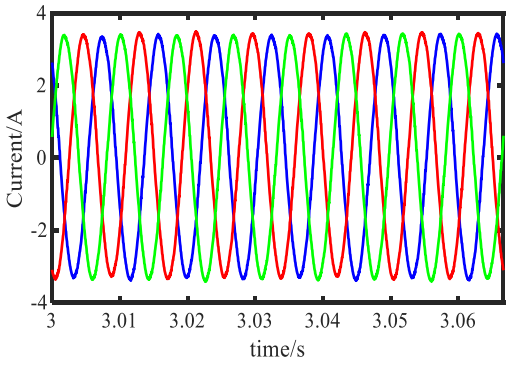

（a）current waveforms

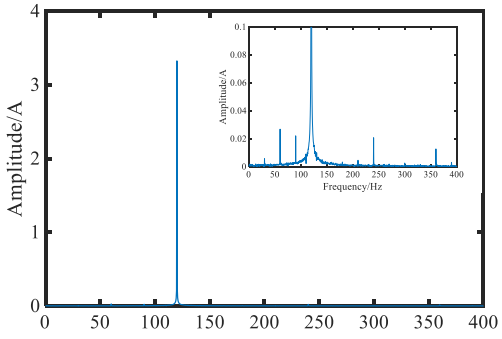

（b）current spectrum-A phase

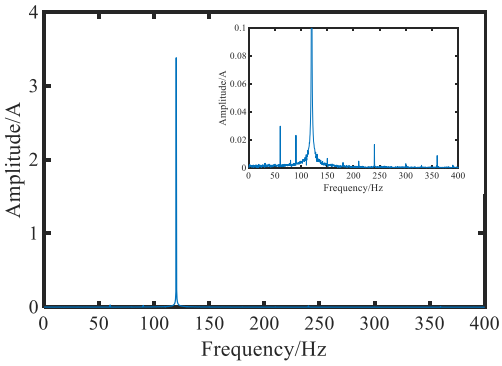

（c）current spectrum-B phase

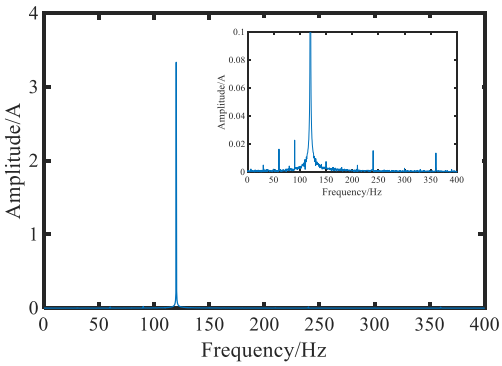

（d）current spectrum-C phase

FIGURE 8. Current waveforms and harmonics of the healthy PMSM.

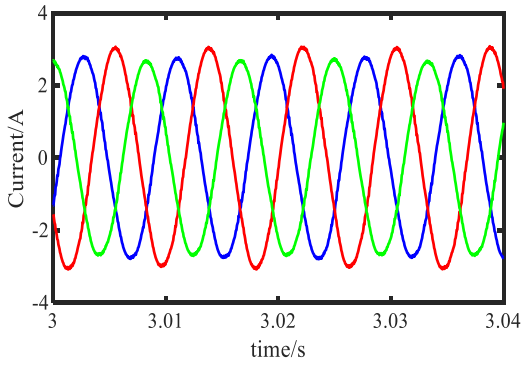

（a）current waveforms

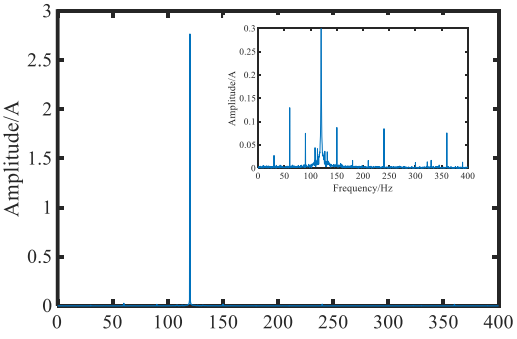

（b）current spectrum-A phase

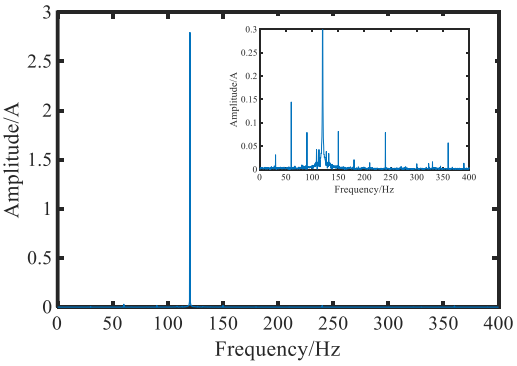

（c）current spectrum-B phase

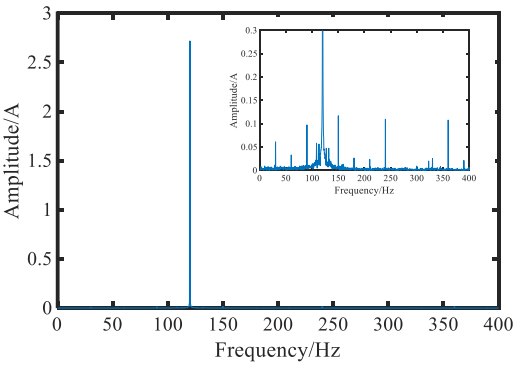

（d）current spectrum-C phase

FIGURE 9. Current waveforms and harmonics obtained from test 2.

current harmonics. In this paper, the normal current waveforms measured at 1800rpm in test 1 are shown in Fig. 8 (a). The current spectrums analyzed with FFT are shown in Fig.8 (b)-(d). The mainly harmonics of stator current are 0.5^{th}(60Hz), 0.45^{th}(90Hz), 2^{nd} (240Hz) and 3^{rd}(360Hz). There are no obvious differences among the three current

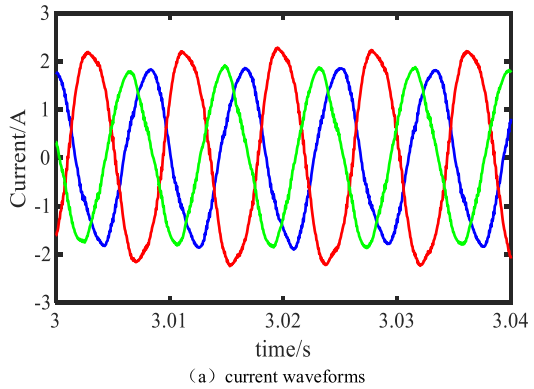

（a）current waveforms

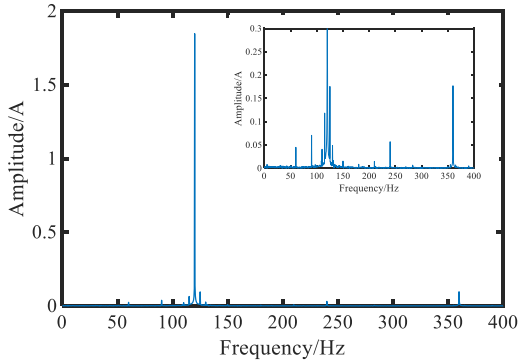

（b）current spectrum-A phase

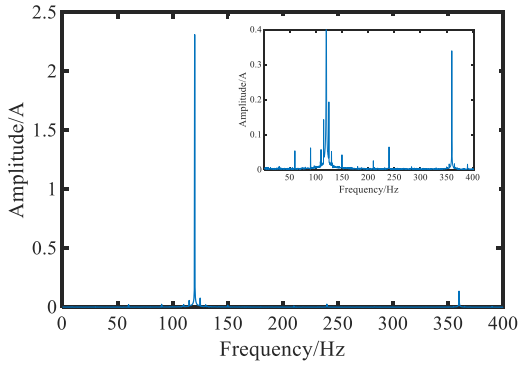

（c）current spectrum-B phase

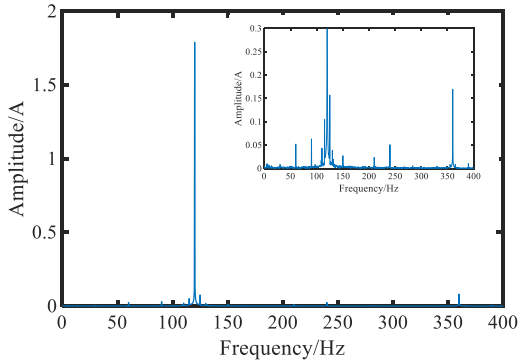

（d）current spectrum-C phase

FIGURE 10. Current waveforms and harmonics obtained from test 3.

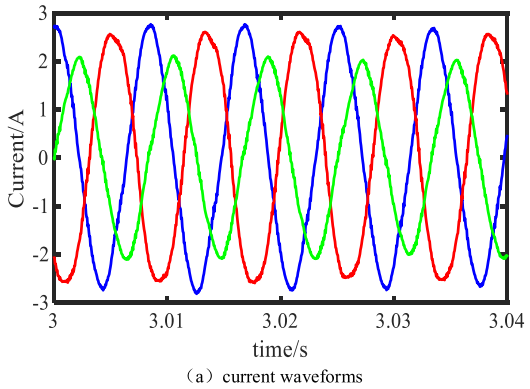

（a）current waveforms

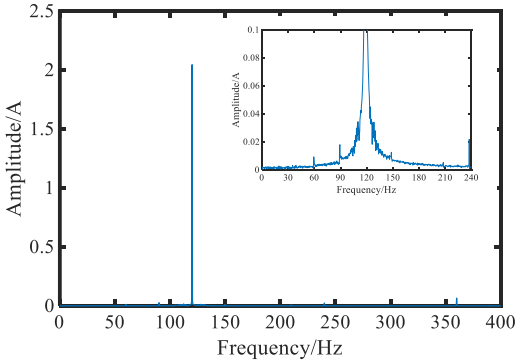

（b）current spectrum-A phase

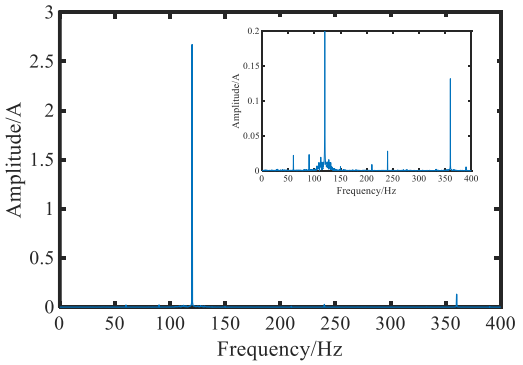

（c）current spectrum-B phase

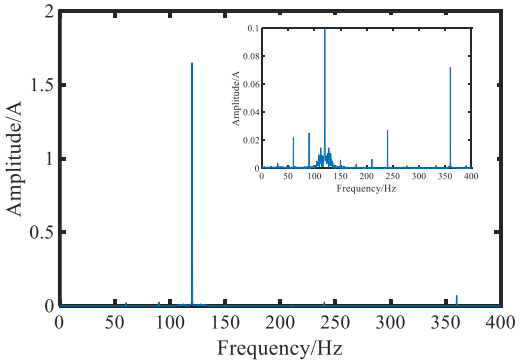

（d）current spectrum-C phase

FIGURE 11. Current waveforms and harmonics obtained from test 4.

spectrums. The testing results from test 2 and 3 are given in Fig. 9 and 10, respectively. By comparison with the results shown in Fig. 8(a), the amplitude of the three phase current waveforms became unequal once the performance of PWM inverter obviously degraded. By comparison with the results shown in Fig. 9(a), it is obviously there are problems of

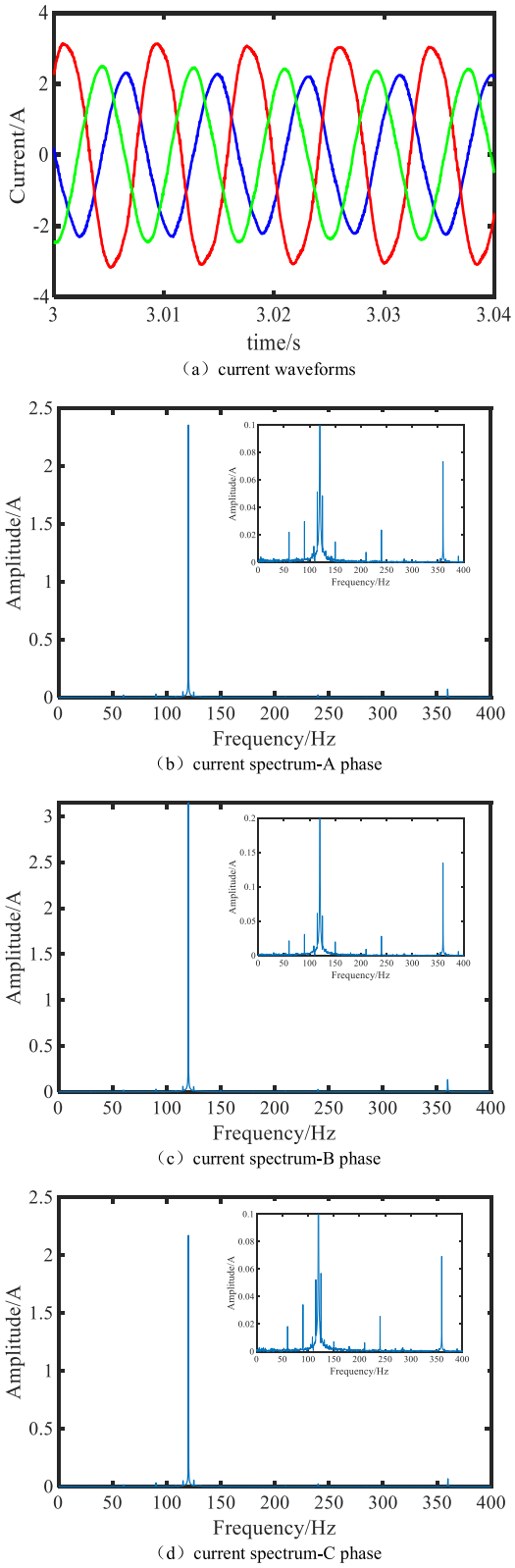

（a）current waveforms
（b）current spectrum-A phase
（c）current spectrum-B phase
（d）current spectrum-C phase

FIGURE 12. Current waveforms and harmonics obtained from test 5.

three-phase asymmetry in Fig. 10(a). Moreover, the amplitude of harmonics increased with performance degradation of PWM inverter. The testing results obtained from test 4 and 5 are given in Fig. 11 and 12, respectively. By comparison with the results shown in Fig. 9 and 10, the problems of three-phase asymmetry became even worse. Furthermore, the amplitude of harmonics was not affected by changing the extent of inter-turn short-circuit.

Overall, both the PWM inverter aging and inter-turn short-circuit resulted in three-phase asymmetry problem and increasing of amplitude of harmonics. The degradation of PWM inverter was not only result in problem of three-phase asymmetry, but also result in increasing of amplitude of harmonics. By contrast, the inter-turn short-circuit more easily lead to problem of three-phase asymmetry. Furthermore, the PWM inverter degradation injection and inter-turn short-circuit injection only changed the amplitude of harmonics, did not change the number of harmonic components.

B. HEALTH INDEX COMPUTATION

As seen in Fig.7 and table 2, by comparison, the amplitude of flux linkage harmonics is close to zero. Therefore, when we estimated the electromagnetic torque by applying (8), we only took into account the 1st (that is k=1) harmonics of flux linkages and 1st, 0.5th, 0.75th, 2nd, 3rd (that is h=1, 0.5, 0.75, 2, 3) harmonics of stator currents. The amplitudes and phase angles of current spectrums obtained from test 1 to 5 are given in table 3. As an example, in what follows, assuming that with the rotor revolving at a constant angular speed and the angle $\Delta\theta$ between the stator flux vector and the rotor flux vector is equal to $\pi/2$ [20]. The computational process of electromagnetic torque by using the measuring flux linkage harmonics and current harmonics are given as following.

As seen in table 3, $i_{a,h}$, $i_{b,h}$ and $i_{c,h}$ are different. By introducing $i_{a,1}$, $i_{b,1}$ and $i_{c,1}$ into T^0 respectively, T_a^0, T_b^0 and T_c^0 can be calculated. For example, by using the data obtained from test 1, the T_a^0, T_b^0 and T_c^0 can be calculated as in Eq. (12):

$$\begin{cases} T_a^0 = 1.5p\psi_1 i_{a,1} = 0.316\text{Nm} \\ T_b^0 = 1.5p\psi_1 i_{b,1} = 0.322\text{Nm} \\ T_c^0 = 1.5p\psi_1 i_{c,1} = 0.322\text{Nm} \end{cases} \tag{12}$$

By introducing the $i_{a,h}$, $i_{b,h}$ and $i_{c,h}$ into Eq.(8) respectively, three different torque $\Delta T_{a,j}^h$, $\Delta T_{b,j}^h$ and $\Delta T_{c,j}^h$ can also be calculated. The j^{th} torque ripple is equal to the sum of vectors of torque ripple considering stator current harmonics and rotor flux harmonics. Take for example, the 0.25th (1-h) torque ripple is equal to the sum of vectors of torque ripple considering 0.75th (h=0.75) stator current harmonics and 1st rotor flux, that can be calculated as in Eq.(13):

$$\begin{cases} T_{a,0.25}^h = 1.5p\psi_1 |i_{a,0.75} e^{j(\pi/2-\varphi_{a,0.75})}| = 0.002\text{Nm} \\ T_{b,0.25}^h = 1.5p\psi_1 |i_{b,0.75} e^{j(\pi/2-\varphi_{b,0.75})}| = 0.002\text{Nm} \\ T_{c,0.25}^h = 1.5p\psi_1 |i_{c,0.75} e^{j(\pi/2-\varphi_{c,0.75})}| = 0.002\text{Nm} \end{cases} \tag{13}$$

The 0.5th(1-h) torque ripple is equal to the sum of vectors of torque ripple considering 0.5th (h=0.5) current harmonics

and 1st rotor flux, that can be calculated as in Eq.(14):

$$\begin{cases} T^h_{a,0.5} = 1.5p\psi_1|i_{a,0.5}e^{j(\pi/2-\varphi_{a,0.5})}| = 0.003\text{Nm} \\ T^h_{b,0.5} = 1.5p\psi_1|i_{b,0.5}e^{j(\pi/2-\varphi_{b,0.5})}| = 0.003\text{Nm} \\ T^h_{c,0.5} = 1.5p\psi_1|i_{c,0.5}e^{j(\pi/2-\varphi_{c,0.5})}| = 0.002\text{Nm} \end{cases} \tag{14}$$

The 1st(1-h) torque ripple is equal to the sum of vectors of torque considering 2nd (h=2) current harmonics and 1st rotor flux, that can be calculated as in Eq. (15):

$$\begin{cases} T^h_{a,1} = 1.5p\psi_1|i_{a,2}e^{j(\pi/2-\varphi_{a,2})}| = 0.000\text{Nm} \\ T^h_{b,1} = 1.5p\psi_1|i_{b,2}e^{j(\pi/2-\varphi_{b,2})}| = 0.002\text{Nm} \\ T^h_{c,1} = 1.5p\psi_1|i_{c,2}e^{j(\pi/2-\varphi_{c,2})}| = 0.001\text{Nm} \end{cases} \tag{15}$$

Similarly, the 2nd torque ripple is equal to the sum of vectors of torque considering 3rd stator current harmonics and 1st rotor flux. The sum of torques are given in Eq. (16):

$$\begin{cases} T_a = T^0_a + \sum\limits_j T^h_{a,j} = 0.321\text{Nm} \\ T_b = T^0_b + \sum\limits_j T^h_{b,j} = 0.330\text{Nm} \\ T_c = T^0_c + \sum\limits_j T^h_{c,j} = 0.324\text{Nm} \end{cases} \tag{16}$$

where $j = 0.25, 0.5, 1, 2$.

By substituting the values of T_a, T_b and T_c into Eq.(10) yields $K_s = 2.9\%$, and substituting the T^0_a, T^0_b and T^0_c into Eq. (10) yields health index $K_0 = 1.8\%$. Meanwhile, the measuring torque ripple ratio K_m is 2.7% by using the torsional sensor. In contrast to measuring K_m, the respectively relative deviation R_s and R_0 are 7.4% and 33.3%, where $R_s = |K_s - K_m|/K_m \times 100\%$ and $R_0 = |K_0 - K_m|/K_m \times 100\%$. Table 4 gives the health indexes and the corresponding deviation obtained from the test. The results show that the K_s is more close to the measuring K_m, and the relative deviation is no more than 10%. That is, the health index K_s calculated by substituting the T_a, T_b and T_c into Eq. (10) is much more satisfactory for monitoring performance degradation of PMSM.

C. PERFORMANCE DEGRADATION ANALYSIS

In test 6, the PMSM was tested until the torque ripple ratio was greater than 20%. After the testing, the changes in current signal are firstly analyzed and the PMSM was disassembled to find the failure cause. As an example, this paper only gives the results measured under 1800rpm and about 70% rated current, which is close to actual conditions. The current waveforms and harmonics are shown in Fig.13. By comparison with the results shown in Fig.8 (a), it is obviously there are three-phase asymmetry problems as shown in Fig.13 (a). The mainly harmonic frequencies are 0.5th(60Hz), 0.45th(90Hz), 2nd (240Hz) and 3rd(360Hz). By comparison with the results shown in Fig.8 (b), (c) and (d), the amplitude of harmonics increased. This indicated the performance of the PMSM degraded significantly by considering the other test results shown in Fig. 9, 10, 11, and 12. The speed response is given in Fig.14. It can be noticed that performance degradation has impact on the speed fluctuation.

TABLE 3. Amplitudes and phase angles of current spectrums.

Test	Phase		h (Hz)				
			0.5(30)	0.75(90)	1(120)	2(240)	3(360)
1	A	$i_{a,h}$	0.027	0.022	3.324	0.001	0.000
		$\varphi_{a,h}$	-0.918	-1.478	0.021	2.912	1.221
	B	$I_{b,h}$	0.030	0.023	3.384	0.017	0.009
		$\varphi_{b,h}$	-3.112	3.071	-1.954	0.836	-1.070
	C	$I_{c,h}$	0.016	0.0228	3.336	0.015	0.014
		$\varphi_{c,h}$	0.790	0.73	1.92	-0.611	0.510
2	A	$i_{a,h}$	0.045	0.071	1.847	0.057	0.177
		$\varphi_{a,h}$	-0.566	-0.174	2.899	-2.76	-0.705
	B	$I_{b,h}$	0.054	0.0642	2.312	0.064	0.339
		$\varphi_{b,h}$	-1.98	-2.8	0.978	2.892	-3.003
	C	$I_{c,h}$	0.52	0.063	1.79	0.051	0.170
		$\varphi_{c,h}$	0.25	1.777	-1.522	-1.289	1.821
3	A	$i_{a,h}$	0.1446	0.08	2.795	0.08	0.0571
		$\varphi_{a,h}$	1.719	0.735	-2.16	-2.719	-1.080
	B	$I_{b,h}$	0.130	0.075	2.76	0.085	0.080
		$\varphi_{b,h}$	-0.618	-1.461	2.01	-1.313	1.032
	C	$I_{c,h}$	0.061	0.100	2.718	0.101	0.108
		$\varphi_{c,h}$	-2.969	2.815	-0.077	0.983	3.051
4	A	$i_{a,h}$	0.020	0.034	2.172	0.026	0.070
		$\varphi_{a,h}$	2.701	2.377	1.611	-2.496	0.870
	B	$I_{b,h}$	0.022	0.031	3.149	0.028	0.135
		$\varphi_{b,h}$	0.322	0.145	-0.69	-0.362	-0.483
	C	$I_{c,h}$	0.022	0.03	2.355	0.024	0.074
		$\varphi_{c,h}$	-2.080	-1.818	-3.010	1.893	-3.017
5	A	$i_{a,h}$	0.073	0.027	2.045	0.024	0.066
		$\varphi_{a,h}$	-1.010	-3.017	2.955	1.610	2.747
	B	$I_{b,h}$	0.022	0.023	2.672	0.028	0.132
		$\varphi_{b,h}$	-3.140	0.550	0.850	-0.276	0.205
	C	$I_{c,h}$	0.022	0.025	1.650	0.027	0.073
		$\varphi_{c,h}$	0.650	2.540	-1.736	-2.767	-2.187

TABLE 4. Torque ripple ratio and its Relative error.

Test	K_0	K_s	K_m	R_0	R_s
1	1.8	2.9	2.7	33.3%	7.4%
2	2.8	3.1	3.2	12.5%	3.1%
3	11.5	17.5	16.1	28.6%	8.7%
4	27.5	26.5	24.1	14.1%	9.9%
5	48.2	45.6	46.3	7.6%	1.5%

The change in torque ripple ratios K_m, health index K_0 and K_s are shown in Fig.15. The relative error R_0 and R_s are shown in Fig.16. The torque ripple ratio presents increasing trend as time goes on. In contrast to the measuring K_0, the K_s is more close to the K_m. The change in health index is consistent with change in the torque ripple ratio. As given in Fig.16, the relative error of K_s is no more than 10% over time, but the relative error of K_0 is much larger with large fluctuations. This indicated the health index K_s can satisfy the need of early performance degradation detecting. Furthermore, the health index maintained at 3.5% until the 35th week. Then, the health index increased as time goes on. Supposing that the threshold value is 3.5%, the performance degradation of the

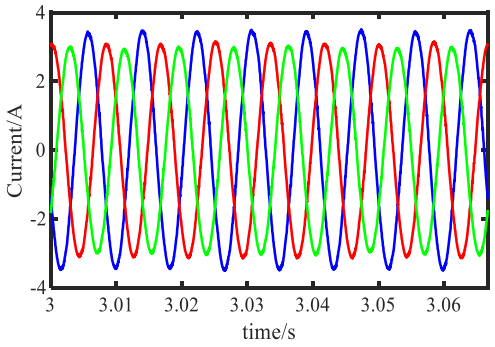

(a) current waveforms

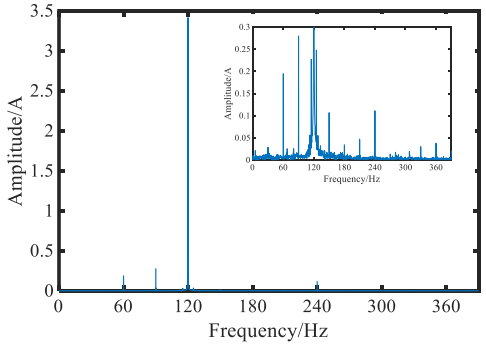

(b) current spectrum-A phase

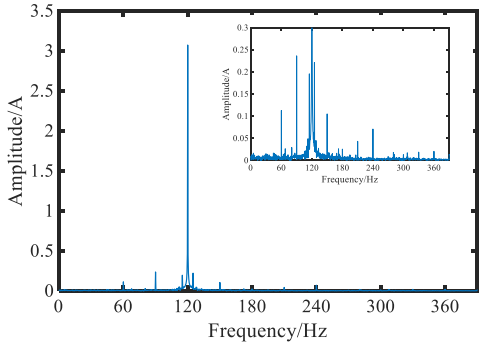

(c) current spectrum-B phase

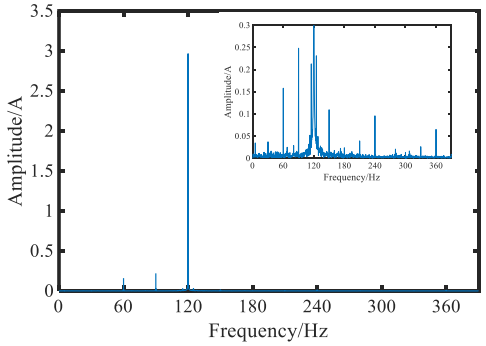

(d) current spectrum-C phase

FIGURE 13. Current waveforms and harmonics obtained from test 6.

PMSM can be identified as long as the health index reaches 3.5%.

The significantly change in health index indicated there was something wrong with the PMSM. As shown in Fig.17,

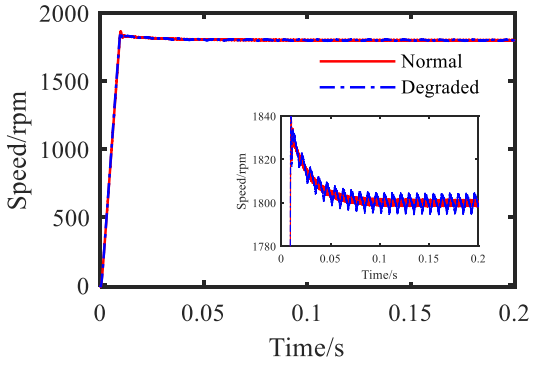

FIGURE 14. Dynamic step speed response at 1800 rpm.

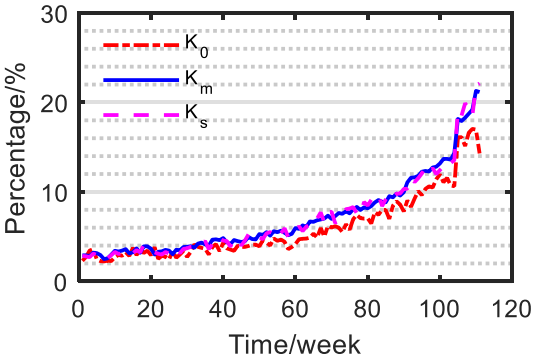

FIGURE 15. Change in the torque ripple ratios.

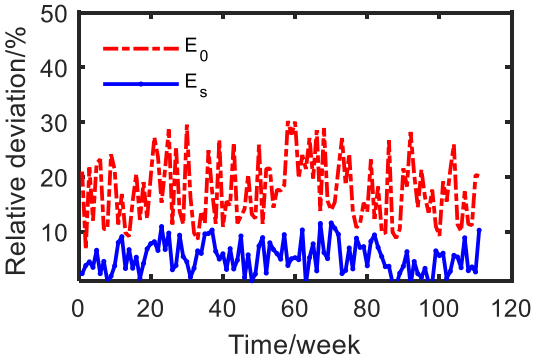

FIGURE 16. Change in the relative error.

we completely disassembled the motor and driver to find the root cause. The encoder is in normal condition. The stator winding resistance (the R_{ab}, R_{bc} and R_{bc}) measured by a digital multimeter are approximately equal. The superficial magnetic field of the rotor measured by a tesla meter demagnetized by only about 3%. The R_{DS} of the MOSFET components decreased by about 8%. The brightness of the bearings has worn off, which resulted in a small eccentricity. Generally, the high temperature produced by large stator currents was the major reason of MOSFET components degradation. The high temperature produced by large stator currents and eddy current loss and also the aging of magnet components itself resulted in demagnetization. MOSFET

components degradation, demagnetization. Long-term use resulted in bearing wear. Mingled and integrated together, all these factors resulted in torque ripple ratio increasing as time goes on. Overall, whatever the reasons for performance degradation, it can result increasing of torque ripple ratio and also the health index K_S. The proposed healthy index K_S can be used to evaluate performance and early identify degradation for the PMSM.

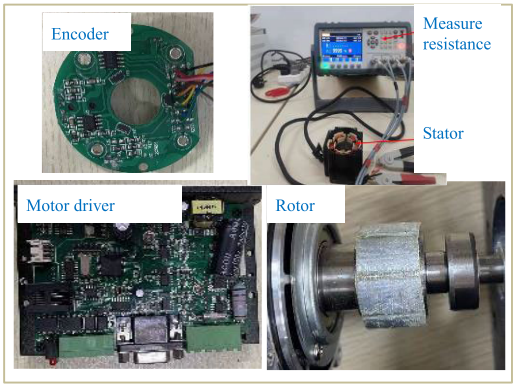

FIGURE 17. Changes of the healthy PMSM torque ripple ratios.

D. DISCUSSION

It is worth noting there are factors causing error in the test result. At present, there is no accurate method to monitor demagnetization during the PMSM is working. We did not monitor the changes in superficial magnetic field until the motor was disassembled. When demagnetization reaches a certain extent the back-emf spectrums changes. We did not identify when the superficial magnetic field of the rotor began to change. Moreover, magnetic saturation is also a potential factor in causing torque ripple in PMSM. The current should be measured under constant speed so that the more accurate and reliable current spectrums can be analyzed with FFT. The results show that the extent of performance degradation can be identified more accurately under constant speed.

Compared to the tested PMSM, the moment of inertia of the magnetic powder brake is much greater. There are speed fluctuations due to stability of load when the magnetic powder brake is used to simulate load. This factor influences the speed control accuracy. This in turn has effects on the waveform of stator current, and even the harmonic components of stator currents. Different factors such as design characteristics, the winding configuration and load level variation, even the torque ripple reduction control methods, have effects on the harmonic components of stator currents. Overall, all the factors should be fully considered when the health index is measured by using the proposed method in this paper.

V. CONCLUSION

This paper proposed a new method with aim to detect early performance degradation and prevent catastrophe failure for PMSM. A theoretical expression of electromagnetic torque was developed by fully taking into account the effects of rotor flux harmonics and current harmonics on electromagnetic torque ripple. and also a method to calculate health index was proposed by considering the different amplitude and frequency of harmonic components in three-phase current. Then, the steps on how to monitor performance and identify degradation early are proposed. Experimental results show that the change in the proposed health index is consistent with change in the torque ripple ratio. The proposed health index can be used to accurately monitor the performance of PMSM under actual working condition. As long as significant changes in health index have taken place, it indicates the performance of PMSM degrades, and there is something wrong with the PMSM. By following the proposed approach, the early performance degradation can be detected in time.

REFERENCES

[1] Y. Chen, S. Liang, W. Li, H. Liang, and C. Wang, "Faults and diagnosis methods of permanent magnet synchronous motors: A review," *Appl. Sci.*, vol. 9, no. 10, p. 2116, May 2019.

[2] J. Faiz and S. A. H. Exiri, "Short-circuit fault diagnosis in permanent magnet synchronous motors—An overview," in *Proc. Optim. Electromotion (ACEMP)*, Side, Turkey, Sep. 2015, pp. 18–27.

[3] J. Rosero, L. Romeral, J. Cusido, and J. A. Ortega, "Fault detection by means of wavelet transform in a PMSMW under demagnetization," in *Proc. 33rd Annu. Conf. IEEE Ind. Electron. Soc. (IECON)*, Taipei, Taiwan, Nov. 2007, pp. 1149–1154.

[4] A. G. Espinosa, J. A. Rosero, J. Cusido, L. Romeral, and J. A. Ortega, "Fault detection by means of Hilbert–Huang transform of the stator current in a PMSM with demagnetization," *IEEE Trans. Energy Convers.*, vol. 56, no. 2, pp. 312–318, Jun. 2010.

[5] J. Rosero, L. Romeral, E. Rosero, and J. Urresty, "Fault detection in dynamic conditions by means of discrete wavelet decomposition for PMSM running under bearing damage," in *Proc. 24th Annu. IEEE Appl. Power Electron. Conf. Expo.*, Washington, DC, USA, Feb. 2009, pp. 951–956.

[6] B. M. Ebrahimi, J. Faiz, and B. N. Araabi, "Pattern identification for eccentricity fault diagnosis in permanent magnet synchronous motors using stator current monitoring," *IET Electr. Power Appl.*, vol. 4, no. 6, p. 418, Nov. 2010.

[7] R. Abdelli, A. Bouzida, O. Touhami, and M. Ouadah, "Static eccentricity fault modeling in permanent-magnet synchronous motors," in *Proc. ICMIC*, Algiers, Algeria, Nov. 2016, pp. 364–368.

[8] H. Liang, Y. Chen, S. Liang, and C. Wang, "Fault detection of stator interturn short-circuit in PMSM on stator current and vibration signal," *Appl. Sci.*, vol. 8, no. 9, p. 1677, Sep. 2018.

[9] E. Elbouchikhi, V. Choqueuse, F. Auger, and M. E. H. Benbouzid, "Motor current signal analysis based on a matched subspace detector," *IEEE Trans. Instrum. Meas.*, vol. 66, no. 12, pp. 3260–3270, Dec. 2017.

[10] J. Urresty, J. Riba, L. Romeral, J. Rosero, and J. Serna, "Stator short circuits detection in PMSM by means of Hilbert–Huang transform and energy calculation," in *Proc. IEEE Int. Symp. Diag. Electric Mach., Power Electron. Drives*, Cargese, France, Aug. 2009, pp. 1–7.

[11] J. Holtz and L. Springob, "Identification and compensation of torque ripple in high-precision permanent magnet motor drives," *IEEE Trans. Ind. Electron.*, vol. 43, no. 2, pp. 309–320, Apr. 1996.

[12] L. Wu and Z. Lyu, "Harmonic injection-based torque ripple reduction of PMSM with improved DC-link voltage utilization," *IEEE Trans. Power Electron.*, vol. 38, no. 7, pp. 7976–7981, Jul. 2023.

[13] K. Xia, J. Lu, B. Dong, K. Xia, X. Yuan, and C. Liu, "A new test system for torque testing and efficiency measurement of three-phase induction motor," in *Proc. 11th Conf. Ind. Electron. Appl. (ICIEA)*, Jun. 2016, pp. 256–261.

[14] K. Xia, M. H. Xu, and C. Bi, "Overview of torque ripple measuring methods for motors," *Electron. Meas. Technol.*, vol. 41, no. 5, pp. 87–94, Apr. 2018.

[15] B. M. Ebrahimi, M. J. Roshtkhari, J. Faiz, and S. V. Khatami, "Advanced eccentricity fault recognition in permanent magnet synchronous motors using stator current signature analysis," *IEEE Trans. Ind. Electron.*, vol. 61, no. 4, pp. 2041–2052, Apr. 2014.
[16] C. Zhu, Z. Zeng, and R. Zhao, "Comprehensive analysis and reduction of torque ripples in three-phase four-switch inverter-fed PMSM drives using space vector pulse-width modulation," *IEEE Trans. Power Electron.*, vol. 32, no. 7, pp. 5411–5424, Jul. 2017.
[17] R. Thike and P. Pillay, "Experimental study of torque-ripple and its effect on the flux weakening range of synchronous reluctance machines," in *Proc. IEEE Int. Electr. Mach. Drives Conf. (IEMDC)*, San Diego, CA, USA, May 2019, pp. 1479–1484.
[18] T. H. Lee, T.-S. Low, K.-J. Tseng, and H. K. Lim, "An intelligent indirect dynamic torque sensor for permanent magnet brushless DC drives," *IEEE Trans. Ind. Electron.*, vol. 41, no. 2, pp. 191–199, Apr. 1994.
[19] D. Zeng, J. Zou, and Y. Xu, "An indirect testing method for the torque ripple of multiunit permanent magnet synchronous machines," *IEEE Trans. Ind. Electron.*, vol. 67, no. 4, pp. 2734–2743, Apr. 2020.
[20] M. Huang, Y. Deng, H. Li, and J. Wang, "Torque ripple attenuation of PMSM using improved robust two-degree-of-freedom controller via extended sliding mode parameter observer," *ISA Trans.*, vol. 129, pp. 558–571, Oct. 2022.
[21] M. Gu, Z. Wang, and B. Wang, "Optimization of torque ripple for low-carrier-ratio dual three-phase PMSM with pulse pattern control," *IEEE Trans. Power Electron.*, vol. 38, no. 12, pp. 15091–15096, Dec. 2023.
[22] R. Krishnan, *Permanent Magnet Synchronous and Brushless DC Motor Drives*, 1st ed. Boca Raton, FL, USA: CRC Press, Oct. 2010.
[23] C. G. Ma, S. G. Zuo, L. C. He, Q. Sun, and Z. Meng, "Analytical calculation of electromagnetic torque in permanent magnet synchronous machine in distributed drive," *J. Vib. Shock*, vol. 32, no. 6, pp. 38–42, Mar. 2013.
[24] S. N. Vukosavic, *Electrical Machines*, 1st ed. Heidelberg, Germany: Springer, Oct. 2012.
[25] J. C. Li and Y. Liao, "Model of permanent magnet synchronous motor considering saturation and rotor flux harmonics," *Proc. CSEE*, vol. 31, no. 3, pp. 60–66, Jan. 2011.
[26] D. P. Zeng, J. B. Zou, and Y. X. Xu, "An indirect testing method for the mechanical characteristic of multiunit permanent-magnet synchronous machines with concentrated windings," *IEEE Trans. Ind. Electron*, vol. 62, no. 12, pp. 7402–7411, Dec. 2015.

QINGCHUAN HE was born in Henan, China, in 1984. He received the Ph.D. degree in reliability engineering from Zhejiang Sci-Tech University, Zhejiang, in 2013. He is currently a Professor Assistant with the National and Local Joint Engineering Research Center of Reliability Analysis and Testing for Mechanical and Electrical Products, Zhejiang Sci-Tech University. His current research interests include reliability design, accelerated life testing, prognostics, and health management of mechanical and electrical products.

JUN PAN was born in Jiangxi, China, in 1974. He received the Ph.D. degree from Zhejiang Sci-Tech University, Hangzhou, China, in 2011. He is currently a Professor with the National and Local Joint Engineering Research Center of Reliability Analysis and Testing for Mechanical and Electrical Products, Zhejiang Sci-Tech University. His current research interests include modeling and statistical analysis of accelerated degradation testing, design of testing plans, reliability estimation, prognostics, and health management.

XIAOTIAN LYU was born in Zhejiang, China, in 1971. She received the bachelor's degree in mechanical design and manufacture from Lishui University, Zhejiang, in 1994. She is currently a Senior Engineer with Zhejiang CHR Intelligent Equipment Company Ltd. Her current research interest includes the reliability design of mechanical and electrical equipment.